

Electro-osmotic properties of porous permeable films

Elena F. Silkina,¹ Naren Bag,² and Olga I. Vinogradova^{1,2,*}

¹*Frumkin Institute of Physical Chemistry and Electrochemistry,*

Russian Academy of Sciences, 31 Leninsky Prospect, 119071 Moscow, Russia

²*DWI - Leibniz Institute for Interactive Materials, Forckenbeckstr. 50, 52056 Aachen, Germany*

(Dated: June 29, 2020)

Permeable porous coatings on a flat solid support significantly impact its electrostatic and electrokinetic properties. Existing work has focused on simplified cases, such as weakly charged and/or thick porous films, with limited theoretical guidance. Here, we consider the general case of coatings of any given volume charge density and obtain analytic formulas for electrostatic potential profiles, valid for any film thickness and salt concentration. Our analysis provides a framework for interpreting and predicting super properties specific to porous films, from an enhanced ion absorption to an amplified electro-osmotic flows due to emergence of slip velocity at interface with an outer electrolyte leading to a large zeta-potential. The latter can be tuned by varying amount of added salt, and remains finite at even high concentrations. The results are relevant for hydrogel coatings, porous carbon and silica, polyelectrolyte brushes, and more.

Charged porous materials that are permeable to water and ions, such as polyelectrolyte networks, ion-exchange resins, silica gels, porous membranes and electrodes, have found use in a large body of applications including water desalination [1], tissue engineering [2, 3], and electrochemical systems [4]. Thanks to a recently discovered extremely strong electrokinetic flow near porous surfaces [5], new opportunities in microfluidics and advanced colloid technologies are emerging. Porous films on a variety of supports, are similarly capable to provide such properties as improved transport and storage capacities for ions, that they did not have when impermeable.

The quantitative understanding of novel equilibrium and transport properties, which could not be achieved without porosity is still challenging. Analytic solutions based on a linearized Poisson-Boltzmann theory are known [6–8], but these results do not apply to highly charged coatings, where nonlinear electrostatic effects could become significant. The non-linear electrostatic problem has been treated using numeric and semi-analytic approaches [6, 9, 10], and some simple expressions for the surface potential, Ψ_s have been derived for thick coatings compared to the Debye screening length, λ_D , which is a measure of the thickness of the electrostatic diffuse layer [6, 11]. There are data indicating that zeta-potential, Z , which is the measure of electrokinetic mobility, can exceed Ψ_s [10, 12], suggesting that porous surfaces can amplify electro-osmotic pumping at micron scales, where pressure-driven flows are suppressed by viscosity. Nevertheless, general principles to control Ψ_s or Z have not yet been established in the case of moderately and, especially, strongly charged coatings, where the implication of porosity is the most pronounced.

In this letter, we describe analytically the distribution of a potential induced by a planar porous coating. Our expressions are valid even when the volume charge density is quite large, and can be used for any salt concentration and thickness of a porous layer. From this theory, we

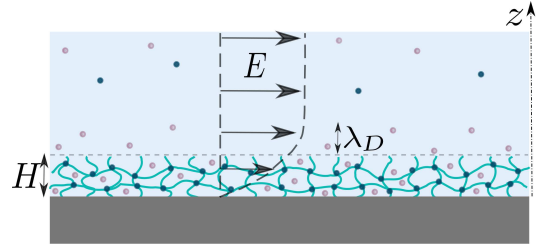


FIG. 1. Porous film of thickness H in contact with an electrolyte solution. Anions and cations are denoted with bright and dark circles. The film is permeable for ions, so that the potential at the support, ψ_0 , and the surface potential, ψ_s , are established self-consistently. An outer electrostatic diffuse layer of a thickness, which is of the order of the Debye screening length, $\lambda_D \equiv \kappa^{-1}$, is formed in the vicinity of the coating. The application of a tangential electric field, E , leads to an electro-osmotic flow of a solvent (shown by arrows).

derive concentration profiles that provide a framework for interpreting absorption properties and boosting storage capacities for ions. We also obtain bounds on attainable electro-osmotic velocity and zeta-potential, and provide guidance for a giant amplification of electro-osmotic flow.

The system geometry is shown in Fig. 1. The permeable film of a thickness H and a fixed volume charge density ρ (taken positive without loss of generality) is placed in an 1:1 electrolyte solution of bulk concentration c_∞ and permittivity ε . Ions obey Boltzmann distribution, $c_\pm(z) = c_\infty \exp(\mp\psi(z))$, where $\psi(z) = e\Psi(z)/(k_B T)$ is the dimensionless electrostatic potential, e is the elementary positive charge, k_B is the Boltzmann constant, T is a temperature, and the upper (lower) sign corresponds to the cations (anions). The inverse Debye screening length of an electrolyte solution, $\kappa \equiv \lambda_D^{-1}$, is defined as usually, $\kappa^2 = 8\pi\ell_B c_\infty$, with the Bjerrum length $\ell_B = \frac{e^2}{\varepsilon k_B T}$.

To calculate the profile of a potential inside the porous film and in the outer solution we employ the nonlinear

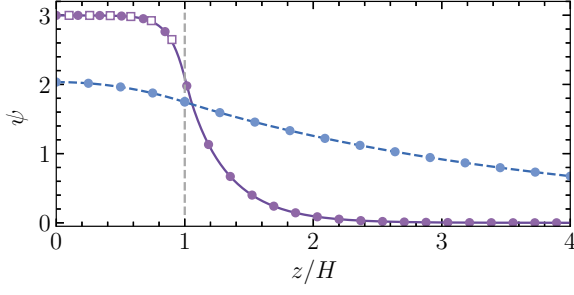


FIG. 2. A distribution of a potential built up by a film of $\rho = 10$, calculated numerically for $\kappa H = 0.3$ (dashed curve) and 3 (solid curve). Filled circles correspond to calculations from Eqs.(11) and (9), when $z/H \leq 1$, and from Eq.(2), when $z/H \geq 1$. Open squares are obtained from Eq.(12).

Poisson-Boltzmann theory [13], so that $\psi(z)$ satisfies

$$\psi''_{i,o} = \kappa^2 (\sinh \psi_{i,o} - \rho \Theta(H - z)), \quad (1)$$

where $'$ denotes d/dz , with the index $\{i, o\}$ standing for “in” ($z \leq H$) and “out” ($z \geq H$), $\rho = \frac{q}{2ec_\infty}$, and the Heaviside step function $\Theta(z)$. The solution of non-linear Eq.(1) with prescribed boundary conditions, in general requires a numerical method. Here we obtain a closed-form analytical solution (see the Supplemental Material [14] for detail). Integrating Eq.(1) twice by applying conditions $\psi'_o \rightarrow 0$ and $\psi_o \rightarrow 0$ at $z \rightarrow \infty$ we naturally find that the ψ_o -profile is identical to derived for a single impenetrable wall [13]

$$\psi_o = 4 \operatorname{artanh} \left[\gamma e^{-\kappa(z-H)} \right] \quad (2)$$

where $\gamma = \tanh \frac{\psi_s}{4}$ and $\psi_s = \psi(H)$ is the surface potential. Using $\psi'_i(0) = 0$ and $\psi_i(0) = \psi_0$ we obtain that for planar films of any thickness ψ_0 and ψ_s are related as

$$\psi_s \equiv \psi_0 - \frac{\cosh \psi_0 - 1}{\rho}, \quad (3)$$

derived before for a limit of thick films only [11].

In the limit of a thin film, $\kappa H \ll 1$, the asymptotic approach suggested before [15] can be employed. Expanding the potential in Eq.(1) about $z = 0$, we obtain, to second order in κz

$$\psi_i(z) \simeq \psi_0 - \frac{\rho}{2} (\kappa z)^2 \left[1 - \frac{\sinh \psi_0}{\rho} \right]. \quad (4)$$

From Eqs.(4) and (3) it follows that ψ_0 satisfies

$$\rho^2 - \rho \sinh \psi_0 - \frac{2(\cosh \psi_0 - 1)}{(\kappa H)^2} \simeq 0, \quad (5)$$

and standard manipulations then yield

$$\psi_0 \simeq \ln \left[\frac{2 + (\rho \kappa H)^2 + \rho \kappa H \sqrt{4 + (\kappa H)^2 (1 + \rho^2)}}{2 + \rho (\kappa H)^2} \right] \quad (6)$$

When $\rho \gg 1$ this may be re-expressed as

$$\psi_0 \simeq 2 \operatorname{arsinh} \left(\frac{\rho \kappa H}{2} \right) - \ln \left(1 + \frac{\rho (\kappa H)^2}{2} \right). \quad (7)$$

For small $\rho \kappa H$, the ψ -profile is almost constant throughout the film,

$$\psi_0 \simeq \psi_s \simeq \rho \kappa H \quad (8)$$

Finally, the inner ψ -profile of a thin film is given by

$$\psi_i(z) \simeq \psi_s - \frac{[\sinh \psi_0 - \rho]}{2} \kappa^2 (H^2 - z^2), \quad (9)$$

where ψ_s and ψ_0 are described by Eqs.(3) and (7).

The startling conclusion from analysis of Eq.(5) is that it is also valid for large κH , i.e. thick films, where the inner region far from the interface may be modeled as electroneutral. Indeed, in this case the last term on its left-hand side becomes very small compared with the first two, and we obtain a well-known for thick films result [6]

$$\psi_0 = \operatorname{arsinh}(\rho) \quad (10)$$

The potential of an electroneutral area is usually referred to as the Donnan potential, ψ_D , so that Eq.(10) relates ψ_D with ρ . However, near the surface electrolyte ions screen volume charges of the coating only partly, and an inner diffuse layer is formed. Since the inverse inner screening length $\kappa_i = \kappa (\cosh \psi_0)^{1/2}$ [7], using Eq.(10) we can obtain $\kappa_i \simeq \kappa (1 + \rho^2)^{1/4}$. This indicates that $\kappa_i \simeq \kappa$ only when $\rho \ll 1$. When $\rho \gg 1$, $\kappa_i \simeq \kappa \sqrt{\rho}$, and the criterion of a thick film can be relaxed to $\kappa H \sqrt{\rho} \gg 1$. Using the symmetry arguments the exact expression for ψ_i could be constructed similarly to Eq.(2) as

$$\psi_0 - \psi_i = 4 \operatorname{artanh} \left[\gamma_i e^{-\kappa_i(H-z)} \right], \quad (11)$$

where $\gamma_i = \tanh \frac{\psi_0 - \psi_s}{4}$ is always smaller than 1/4 [14]. Thus, we might argue that for any, even very large ρ , a sensible approximation for the inner potential should be

$$\psi_i(z) \simeq \psi_0 + (\psi_s - \psi_0) e^{\kappa_i(z-H)} \quad (12)$$

This derivation differs from conventional arguments, which assume low volume charge density [6].

In order to assess the validity of the above approach, we employ numerical simulations. Details of calculations are given in the Supplemental Material [14].

In Fig. 2 we plot $\psi(z/H)$ computed for two different values of κH that are close to limits of thick and thin films, and a large fixed ρ . The form of the ψ -profile depends on κH . For $\kappa H = 3$ the inner potential shows a distinct plateau indicating that the intrinsic charge of the film is completely screened by electrolyte ions, i.e. global electroneutrality. The plateau potential is equal

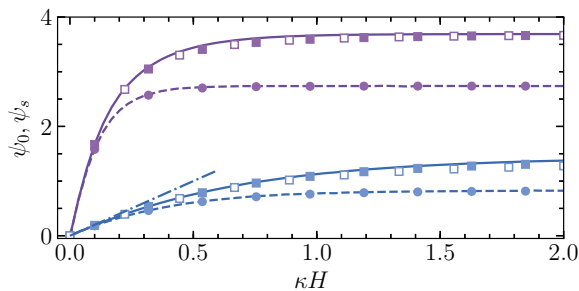


FIG. 3. Potentials at wall (solid lines) and surface (dashed) as a function of κH computed for fixed $\rho = 20$ (upper set of curves) and $\rho = 2$ (lower curves). Filled squares illustrate calculations from Eq.(6), circles are then obtained using Eq.(3). Open squares show results obtained using Eq.(7). Dash-dotted line is calculated from Eq.(8).

to ψ_D . However, when $\kappa H = 0.3$, there is no electroneutral region inside the film, and the potential at wall, ψ_0 , is much smaller than ψ_D . Also included in Fig. 2 are theoretical results obtained from Eqs.(3), (10), (6), and we conclude that in relevant areas they are in excellent agreement with numerical data.

It is tempting to speculate that Eq.(6) will be applicable for any κH , and that a more elegant result, Eq.(7), can be used provided ρ large enough. Clearly, Eq.(5) could become less accurate for intermediate κH , and it is of considerable interest to determine its regime of validity. To test ansatz Eq.(5), numerical and theoretical ψ_0 and ψ_s have been calculated as a function of κH for different values of ρ . Specimen results are plotted in Fig. 3 confirming the validity of Eqs.(6) and (7) for all κH . As expected, Eq.(8), which can also be obtained using the linear theory [6], is valid only when $\rho\kappa H$ is very small and significantly overestimates potentials, which saturate at some κH , in other cases. The charge density dependence of ψ_0 and ψ_s is also of interest. Fig. 4 illustrates the weak growth of both potentials with ρ , and that $\psi_0 - \psi_s \simeq 1$ as $\rho\kappa H$ is increased. We again conclude that Eq.(6) fits accurately the numerical data. So does (7), except for $\rho \leq 1$, where some very small discrepancy is observed. Below we use Eq.(7) for all calculations, by omitting a discussion of the accuracy of our theory.

We make use of results presented above to predict and/or interpret some static and dynamic properties of porous films. One problem for which our analysis is relevant is the concentration of ions in an inner solution that is confined in porous media. In the Supplemental Material [14] we show that in the coating anions are significantly enriched, and cations are depleted, and discuss the degree of this enrichment and depletion depending on ρ and κH .

Another example for which our results are relevant is an electro-osmotic flow of a solvent of the dynamic

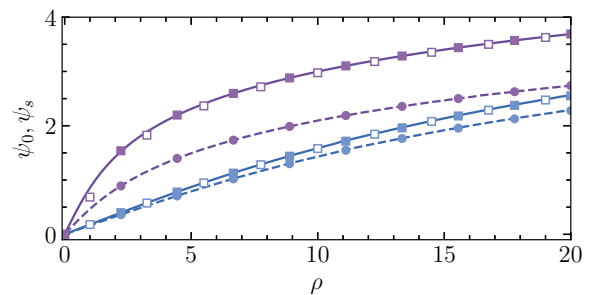


FIG. 4. Potentials at wall (solid lines) and surface (dashed) as a function of ρ computed for fixed $\kappa H = 3$ (upper set of curves) and $\kappa H = 0.2$ (lower curves). Filled squares illustrate calculations from Eq.(6), circles are then obtained using Eq.(3). Open squares show predictions of Eq.(7).

viscosity η in an applied tangential electric field, E . We are now about to relate the dimensionless velocity, $v(z) = \frac{4\pi\ell_B\eta}{eE}V(z)$, of such a flow to ψ_0 and ψ_s . We assume weak field $|E|L \ll |\psi|$, so that in steady state $\psi(z)$ is independent of the fluid flow over a characteristic length L , and neglect surface conduction (which tends to reduce electro-osmotic flow) compared with bulk conduction. Thus, the liquid flow satisfies the generalized Stokes equation

$$v'' - \mathcal{K}^2 v \Theta(H - z) = \psi'' + \kappa^2 \rho \Theta(H - z), \quad (13)$$

with the Darcy-Brinkman correction for an inner flow, where \mathcal{K} is the inverse Brinkman length. At the wall we apply a classical no-slip condition, $v_0 = v(0) = 0$, and far from the surface $v'_{z \rightarrow \infty} = 0$. To obtain bounds on the electro-osmotic velocity for arbitrary porous films with given ρ , we consider the limits of small flow extension into the porous medium, $\mathcal{K}H \rightarrow \infty$, and of $\mathcal{K}H \rightarrow 0$, where an additional dissipation in the porous film can be neglected. These bounds constrain the attainable electro-osmotic velocity and could provide theoretical guidance for porous film and electrolyte solution optimization.

From analysis of Eq.(13) it follows that the outer v -profile and velocity in the bulk are given by

$$v_o(z) = v_\infty + \psi_o(z), \quad v_\infty = v_s - \psi_s = -\zeta, \quad (14)$$

where ψ_o is defined by Eq.(2), $v_s = v(H)$ is the liquid velocity at surface, below we refer it to as slip velocity, and $\zeta = eZ/(k_B T)$. Eqs.(14) indicate that enhanced electro-osmotic mobility can be a consequence of large equilibrium ψ_s , as well as of large v_s that depends on a hydrodynamic permeability of the coating. The amplification of the electro-osmotic flow (compared to the no-slip case with the same ψ_s) can be expressed as

$$\frac{\zeta}{\psi_s} = 1 - \frac{v_s}{\psi_s} \quad (15)$$

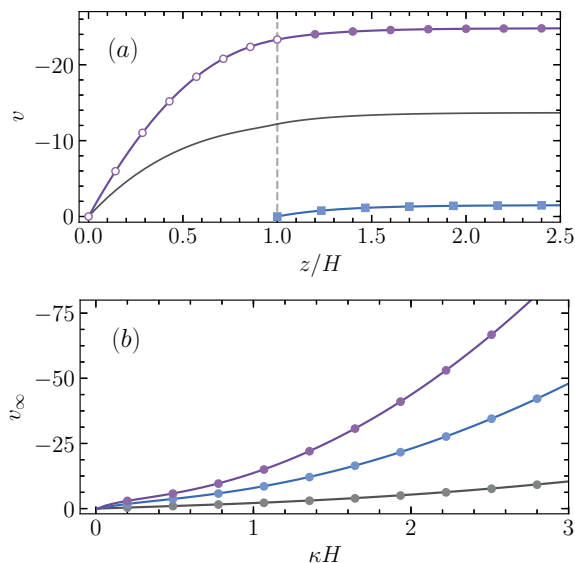


FIG. 5. (a) Electroosmotic velocity profiles computed using $\kappa H = 3$, $\rho = 5$, and $\mathcal{K}H = 0, 1.5$, and ∞ (solid curves from top to bottom). Filled and open symbols indicate calculations from Eqs. (14) and Eq. (16). Squares are obtained using $v_s = 0$, circles correspond to $v_s = \psi_s + v_\infty$, where v_∞ is given by Eq. (17); (b) Computed upper bounds ($\mathcal{K}H \rightarrow 0$) on v_∞ vs. κH (solid curves). From top to bottom $\rho = 20, 10$, and 2 . Circles show results of calculations from Eq.(17).

The problem, thus, reduces to calculation of v_s .

If we suppose $\mathcal{K}H \rightarrow \infty$, the slip velocity nearly vanishes, $\psi_s \simeq \zeta$, and $v_\infty \simeq -\psi_s$, which is equivalent to the Smoluchowsky result. Fig. 5(a) includes typical numerical and theoretical v -profiles calculated for this case using $\kappa H = 3$ and $\rho = 5$ that leads to $\psi_s \simeq 1.5$. When $\mathcal{K}H \rightarrow 0$, integrating Eq.(13) twice, and imposing the continuity of v and v' at $z = H$, we find

$$v_i \simeq (\psi_i - \psi_0) - \rho \kappa^2 \left(H z - \frac{z^2}{2} \right) \quad (16)$$

The outer velocity v_o is given by Eqs.(14) with

$$v_\infty \simeq - \left(\psi_0 + \frac{\rho(\kappa H)^2}{2} \right) \simeq -\zeta \quad (17)$$

The v -profile for this case is also shown in Fig. 5(a). It turns out that even at moderate ρ and κH one can induce significantly (here an order of magnitude) enhanced, compared to the Smoluchowsky case, v_∞ , which is associated with the emergence of a large slip velocity, v_s . Also included in Fig. 5(a) is the curve computed using $\mathcal{K}H = 1.5$, which is located between two limiting cases and demonstrates quite large v_s .

We now verify Eq.(17) and plot theoretical v_∞ vs. κH in Fig. 5(b) together with numerical data. Upon increasing κH at fixed ρ the amplitude of v_∞ grows nonlinearly,

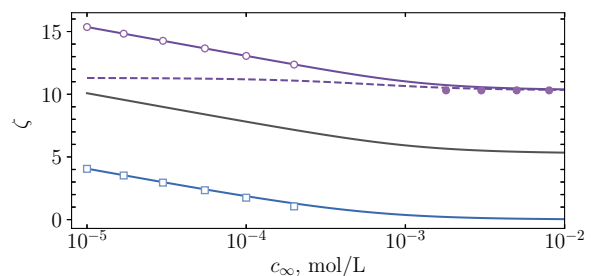


FIG. 6. ζ as a function of c_∞ computed for a film of $H = 50$ nm, $\rho = 150$ kC/m³, using $\mathcal{K}H = 0, 1.5$, and ∞ (solid curves from top to bottom). Dashed curve shows $|v_s|$ at $\mathcal{K}H = 0$. Squares, open and filled circles plot results of calculations from Eqs.(18), (19), and (20).

and in the case of $\rho \gg 1$ becomes several tens of times faster compared to a no-slip case, even at moderate κH . It is tempting to speculate that one can further amplify v_∞ making porous film thicker. However, when the film becomes thick enough, the condition $\mathcal{K}H \rightarrow 0$ violates, and Eq.(17) is no longer valid.

This implies that mobile ions absorbed within the porous layer actively participate in the flow-driving mechanism by reacting to the field. The porous film acts as a charged immobile surface layer with absorbed mobile ions of the opposite sign, but note the difference from a known example of mobile surface charges at slippery wall [16]. In the latter case, slippage is of a hydrodynamic origin and mobile surface charges induce a backward flow, reducing the amplification of electro-osmotic flow caused by hydrodynamic slip. By contrast, in the current work an inner solvent flow induces a forward flow and v_s itself. However, similarly to hydrophobic electrokinetics [16, 17], our large ζ no longer reflects the sole ψ_s . Finally, we would like to stress that a massive amplification of electro-osmotic flow that can be achieved near porous surfaces is of the same order of that at charged super-hydrophobic surfaces [18], and such a fast flow is in agreement with recent observations [5].

So far we have considered the potentials and electro-osmotic velocity at fixed dimensionless ρ and κH . Additional insight into the problem can be gleaned by calculating an upper bound on ζ as a function of $c_\infty \propto \kappa^2$ at fixed H and ρ . Let us now keep fixed $H = 50$ nm and $\rho = 150$ kC/m³, usually referred to as ‘moderate’ [19], and vary c_∞ from 10^{-5} to 10^{-2} mol/L. Upon increasing c_∞ in this range, κH is increased from about 0.5 to 16, and ρ is reduced from about 78 down to 0.1. Therefore, for a given film the required regimes (of thin and thick films, or highly and weakly charged coatings) can be tuned simply by adjusting the concentration of salt in the bulk.

The bounds on attainable ζ are shown by lower and

upper curves in Fig. 6. If $\mathcal{KH} \rightarrow \infty$, $\zeta \simeq \psi_s$ decays from ca. 5 ($Z \simeq 125$ mV) practically to zero as c_∞ increases, leading to a suppression of a flow. In dilute solutions the lower bound on ζ is given by [14]

$$\zeta \simeq \ln\left(\frac{\rho}{ec_\infty}\right) - 1, \quad (18)$$

which perfectly fits numerical data. When $\mathcal{KH} \rightarrow 0$, ζ becomes much larger. Thus, with our smallest concentration $\zeta \simeq 15$ (or $Z \simeq 375$ mV). In a dilute solution [14]

$$\zeta \simeq \ln\left(\frac{\rho}{ec_\infty}\right) + \frac{2\pi\ell_B\rho H^2}{e}, \quad (19)$$

where first term is associated with the potential at the wall. Note that such a logarithmic decay fits reasonably well the obtained for real porous materials electrokinetic data [5]. For concentrated solutions a large, and independent on salt, zeta-potential is observed. The computed slip velocity, also included in Fig. 6, indicates that this occurs when $\zeta \simeq -v_s$ and $\psi_s \simeq 0$. Thus, a large zeta-potential emerges solely due to absorbed ions that generate a forward electro-osmotic flow inside a porous film. It is easy to show that it is given by [14]

$$\zeta \simeq \frac{2\pi\ell_B\rho H^2}{e}, \quad (20)$$

that clarifies the status of second term in Eq.(19). This result is relevant for the understanding zeta-potential measurements with ‘hairy’ surfaces, where it remains finite at even high salt concentrations [20]. We recall that Eqs.(18) and (19) represent the lower and upper bounds for ζ attained at limiting values of \mathcal{KH} . Any finite \mathcal{KH} would lead to ζ confined between the above bounds, as seen in Fig. 6, where we use $\mathcal{KH} = 1.5$.

In summary, our simple analytic equations, obtained within a nonlinear model, provide considerable insight into the electro-osmotic equilibria and flows in the presence of porous coatings. Our theory describes absorption capacity of porous films, which is, in turn, responsible for an enhanced electroosmotic flow. The rigorous bounds on the velocity of electro-osmotic flow we have derived can guide the design of coatings to amplify a variety of electrokinetic phenomena, including streaming current and diffusio-osmosis. Our work clarifies the nature of possible electro-osmotic flow enhancement and makes connection between Brinkman lengths and surface electrokinetic slip. The bounds we obtained constrain the attainable ζ , and it appears timely to derive expressions for an arbitrary \mathcal{KH} , as well as to relate \mathcal{K} with the texture parameters of coatings.

We thank E.S.Asmolov for helpful discussions. This work was supported by the Ministry of Science and Higher Education of the Russian Federation and by the

German Research Foundation (grant Vi 243/4-2) within the Priority Programme ‘‘Microswimmers - From Single Particle Motion to Collective Behaviour’’ (SPP 1726).

* Corresponding author: oivinograd@yahoo.com

- [1] S. Porada, L. Weinstein, R. Dash, A. van der Wal, M. Bryjak, Y. Gogotsi, and P. M. Biesheuvel, *ACS Appl. Mater. Interfaces* **4**, 1194 (2012).
- [2] D. F. Stamatialis, B. J. Papenburg, M. Gironas, S. Saiful, S. N. Bettahalli, S. Schmitmeier, and M. Wessling, *J. Membrane Sci.* **308**, 1 (2008).
- [3] H. H. Chung, M. Mireles, B. J. Kwarta, and T. R. Gaborski, *Lab on a Chip* **18**, 1671 (2018).
- [4] P. M. Biesheuvel, Y. Fu, and M. Z. Bazant, *Phys. Rev. E* **83**, 061507 (2011).
- [5] D. Feldmann, P. Arya, T. Y. Molotilin, N. Lomadze, A. Kopyshchev, O. I. Vinogradova, and S. A. Santer, *Langmuir* **36**, <https://doi.org/10.1021/acs.langmuir.9b03270> (2020).
- [6] H. Ohshima and S. Ohki, *Biophys. J.* **47**, 673 (1985).
- [7] H. Ohshima and T. Kondo, *Biophys. Chem.* **38**, 117 (1990).
- [8] S. Chanda, S. Sinha, and S. Das, *Soft Matter* **10**, 7558 (2014).
- [9] J. F. Duval, *Langmuir* **21**, 3247 (2005).
- [10] G. Chen and S. Das, *J. Colloid Interface Sci* **445**, 357 (2015).
- [11] E. F. Silkina, T. Y. Molotilin, S. R. Maduar, and O. I. Vinogradova, *Soft Matter* **16**, 929 (2020).
- [12] V. D. Sobolev, A. N. Filippov, T. A. Vorob’eva, and I. P. Sergeeva, *Colloid J.* **79**, 677 (2017).
- [13] D. Andelman, *Handbook of biological physics* **1**, 603 (1995).
- [14] See Supplemental Material at [URL will be inserted by publisher] for a derivation of Eqs.(2), (3), (11), (18)-(20) and details of numerical calculations. The Supplemental Material includes Refs. [21–24].
- [15] E. F. Silkina, E. S. Asmolov, and O. I. Vinogradova, *Phys. Chem. Chem. Phys.* **21**, 23036 (2019).
- [16] S. R. Maduar, A. V. Belyaev, V. Lobaskin, and O. I. Vinogradova, *Phys. Rev. Lett.* **114**, 118301 (2015).
- [17] L. Joly, C. Ybert, E. Trizac, and L. Bocquet, *Phys. Rev. Lett.* **93**, 257805 (2004).
- [18] A. V. Belyaev and O. I. Vinogradova, *Phys. Rev. Lett.* **107**, 098301 (2011).
- [19] J. F. Duval, R. Zimmermann, A. L. Cordeiro, N. Rein, and C. Werner, *Langmuir* **25**, 10691 (2009).
- [20] A. Garg, C. A. Cartier, K. J. M. Bishop, and D. Velegol, *Langmuir* **32**, 11837 (2016).
- [21] G. Bader and U. Ascher, *SIAM J. Sci. and Stat. Comput.* **8**, 483 (1987).
- [22] L. Braeken, B. Bettens, K. Boussu, P. Van der Meeren, J. Cocquyt, J. Vermant, and B. Van der Bruggen, *J. Membr. Sci.* **279**, 311 (2006).
- [23] J. Benavente, V. Silva, P. Prádanos, L. Palacio, A. Hernández, and G. Jonson, *Langmuir* **26**, 11841 (2010).
- [24] R. Schweiss, P. B. Welzel, C. Werner, and W. Knoll, *Colloids Surf. A Physicochem. Eng. Asp.* **195**, 97 (2001).